Nonlinear focusing by residual-gas ionization in long-pulse electron linacs

Bruce E. Carlsten
Los Alamos National Laboratory, Los Alamos, New Mexico 87544
(Received 19 March 2001; published 20 September 2001)

For short electron bunches in accelerators, the radial ion density due to residual-gas ionization faithfully reproduces the radial electron bunch distribution for time scales similar to the electron bunch length. If the electron bunch length is sufficiently long, however, the ions focus and, even for radially uniform electron beams, tend to form a very nonuniform equilibrium distribution. This ion distribution, in turn, leads to nonlinear focusing forces on the electron bunch itself. In this paper, we find the equilibrium distribution when the electron distribution is uniform, and calculate the emittance growth for axial slices in the electron bunch later in time. A regime is found in which the emittance growth is quadratic with both residual gas pressure and electron bunch length.

DOI: 10.1103/PhysRevE.64.046501 PACS number(s): 29.27.−a

I. INTRODUCTION

It has been widely recognized that the ion-hose instability in long-pulse electron linear accelerators and short-pulse electron rings can lead to anomalous centroid steering of the electron bunch and beam quality degradation, where the ions are produced by impact ionization of residual gas in the accelerator [1–5]. It is also widely known that ionization of the residual gas will lead to fractional neutralization of the space-charge force of the electron beam [6]. This neutralization fraction is a function of time, and builds up from zero to some final value at the end of the electron bunch, leading to time-dependent focusing and beam quality degradation. This effect is particularly important for relativistic beams, where the forces from the beam's own electric field and magnetic field cancel to order $1/\gamma^2$, where γ is the usual relativistic mass factor. For electron pulses short compared to the oscillation time of ions in the beam's potential well (typically on the order of hundreds of nsec), the physical picture of the time-varying focusing is simple, since the ions can be assumed to stay at rest. For this case, at a given axial position, the fractional ionization radial density profile is the same as the electron beam's, and increases linearly with time. If the electron beam has uniform density, the resulting space-charge force remains linear, and this effect is simple to model [6].

This effect is significantly more complex if the electron bunch length is long compared to the ion oscillation period. The ions now move radially in the beam's potential well, and lead to additional nonlinear effects. The ions are accelerated toward the beam's axis, and lead to a distribution that is peaked on axis. Thus even if the initial electron beam's profile is uniform, the additional space-charge force from the ions will be nonlinear, leading to additional beam quality degradation. It is precisely this effect which we will describe in this paper. We will show that an equilibrium profile shape of the ions is reached after a few oscillation periods (although the magnitude will increase linearly over time). This effect has important consequences for an emerging class of long-pulse induction linear accelerators [7].

A particle-in-cell model of the ions, coupled to an electron particle-in-cell transport code, will be used to calculate this effect for both short and long electron bunches. In Sec. II, we find the equilibrium ion density for an initially uniform density electron bunch both numerically and analytically. We find that the equilibrium distribution shape is attained after only a couple of ion oscillation periods.

In Sec. III, we calculate the emittance growth of an initially cold, uniform density electron bunch as it passes through a thin region with residual gas. The emittance growth is linear with pressure and overall electron bunch length. Then we calculate the emittance growth through long regions, and find that the emittance growth is quadratic with pressure and bunch length when this effect is coupled with emittance oscillations that often occur in high-brightness electron accelerators. We conclude with some simulations of the dual axis radiographic hydrodynamics test (DARHT) long-pulse accelerator [7], which also demonstrate the quadratic scaling of the emittance growth.

II. ION MOTION

In this section, we analyze ion motion within an electron beam. We derive an expression for the equilibrium distribution, and verify it with particle simulations. The equilibrium distribution is highly peaked along the axis of symmetry.

Ions are produced by primary impact ionization of the high-energy electron bunch through low-pressure residual gas. This gas is often composed of air components (N_2, O_2, CO, CO_2, and so on) and hydrocarbons from vacuum pump oil. The exact constituents can be determined by residual gas analyzer measurements, but do not significantly modify the results described in this paper. The ion density produced by primary impact ionization is given by this rate equation [6]

$$\frac{dn_i}{dt} = n_g n_e \sigma \nu, \tag{1}$$

where n_i is the ion density, n_g is the initial gas density (assumed to be uniform over radial distances), n_e is the electron bunch density (which is a function of time at a given axial and radial position), σ is the cross section, and ν is the velocity of the electron bunch (which we will assume to be the

speed of light c). For a temporally uniform electron beam, the fractional ionization is then given by

$$\frac{n_i}{n_e} = n_g \sigma \nu t = \sigma t P_g \ (\text{torr}) 9.783(10^{26}) \ \ \text{cm}^{-2} \ \ \text{sec}^{-1}, \quad (2)$$

where P_g is the gas pressure in torr, at a time t from the head of the electron pulse.

If the electron bunch density is uniform, n_e is independent of radius r, and ions are created uniformly across the electron bunch cross section. If the electron bunch is very short, these ions do not move appreciably while the rest of the beam is passing by. However, if the electron bunch length is long, there can be a redistribution of the ions.

The motion of the ions is dominated by the electric field of the electron bunch—the density ratio of the ions to the electron bunch is typically on the order of 0.001 or less. Thus the self field of the ions can be ignored for their own motion. However, due to the relativistic cancellation of the electron beam's space-charge force on itself, the ions' space charge force on the electrons begin to dominate even at energies as low at 15 MeV, for fractional ionizations of 0.001. The radial equation of motion for the ions in an electric field produced by a uniform density electron bunch is

$$\ddot{r} + r \frac{eI}{2 m_i \varepsilon_0 c \pi a^2} = 0, \quad (3)$$

where e is the electronic charge, I is the instantaneous current of the electron bunch, m_i is the mass of the ions, ε_0 is the permittivity of free space, a is the electron bunch edge radius, and a dot indicates a time derivative. If the electron bunch is axially uniform, the ions will radially oscillate harmonically, with period

$$\tau_{\text{ions}} = \left(\frac{8 m_i \varepsilon_0 c \pi^3 a^2}{eI} \right)^{1/2}. \quad (4)$$

The period of the oscillation for a hydrogen atom in a 3-cm radius, 2-kA electron beam is 55.6 nsec. The ions' self-fields have been neglected in Eqs. (3) and (4), which is consistent with low fractional ionizations. This assumption will lead to a singularity at the origin at a quarter oscillation period which, under the influence of the ions' space charge will tend to smear the distribution. However, for low fractional ionizations, the smearing will be small, and this assumption is not limiting for the case we are interested in.

Ions produced at the same time will stay in phase with these oscillations with these assumptions. Consider some ions produced at some time t. Initially, their distribution is uniform, out to radius a. As they oscillate toward the origin, they stay uniform in density, but with density increasing as a^2/r_e^2, where r_e is the instantaneous edge radius of the distribution. The equation of motion for the edge radius is given by

$$\begin{aligned} r_e &= a \cos \omega t, \\ \dot{r}_e &= -a \omega \sin \omega t, \end{aligned} \quad (5)$$

where the frequency is given by $\omega = \sqrt{eI/2 m_i \varepsilon_0 c \pi a^2}$.

At long times, the equilibrium distribution will be formed by an infinite sum of such distributions, all starting at different times. We can find the functional form of the equilibrium distribution by integrating over starting times. Because of symmetry, we only need to consider initial phases from 0 to $\pi/2$ radians. The radial equilibrium distribution function is then of the form

$$f_{\text{eq}}(r) \propto \int_0^{\theta_{\max}} \frac{d\theta}{a^2 \cos^2 \theta}, \quad (6)$$

where $\theta_{\max}$ is the phase at which the distribution edge is at radius r, and is given by $r = a \cos \theta_{\max}$. After integration, we find

$$f_{\text{eq}}(r) = k \frac{\sqrt{a^2 - r^2}}{r}, \quad (7)$$

where k is some unknown constant, which can be found from conservation of the total number of ions. After comparison to the rate equation [Eq. (1)], the equilibrium distribution is determined to be

$$f_{\text{eq}}(r,t) = \frac{4 n_e n_g \sigma c}{\pi a^2} \frac{\sqrt{a^2 - r^2}}{r} t. \quad (8)$$

We can verify that this is the equilibrium distribution by direct particle-in-cell simulations of the ion motion using the code SLICE [8–10]. The SLICE code self-consistently pushes particles along an induction linac using the Lorentz force equation, including the beam's self-radial electric, axial magnetic, and azimuthal magnetic fields and all external fields to fourth order in radius. The code uses the long-beam approximation, in which Gauss' law is used for the radial electric field and Ampere's law is used for the azimuthal and axial magnetic fields. A collection of particles is used to describe the beam at each axial position.

For long-pulse ionization simulations, at each axial location, the electron beam is separated into discrete time slices. At each time slice, a new ion density is produced on a background grid [following Eq. (1)], and evolved using the electron beam's radial electric field. The precise dynamics of only the first and last electron slices are calculated. The density of intermediate electron slices is assumed to be a linear interpolation of these two slices, which is consistent with a first-order perturbative solution. The last electron slice is influenced by the electric field of the overall ion distribution at its time. In particular, ion density is deposited on 100 radial grid points at each time slice as separate ion macroparticles. Typical long-pulse simulations require 100–10 000 time slices to resolve the ion oscillations in the potential well of the electric beam, requiring 10^4–10^6 ion macroparticles in all, for every axial position in the linac.

Because an equilibrium distribution is attained, a fluid model for the ion distribution would have been sufficient. However, the macroparticle model is easier to make accurate for simulations of ion distributions that oscillate about the

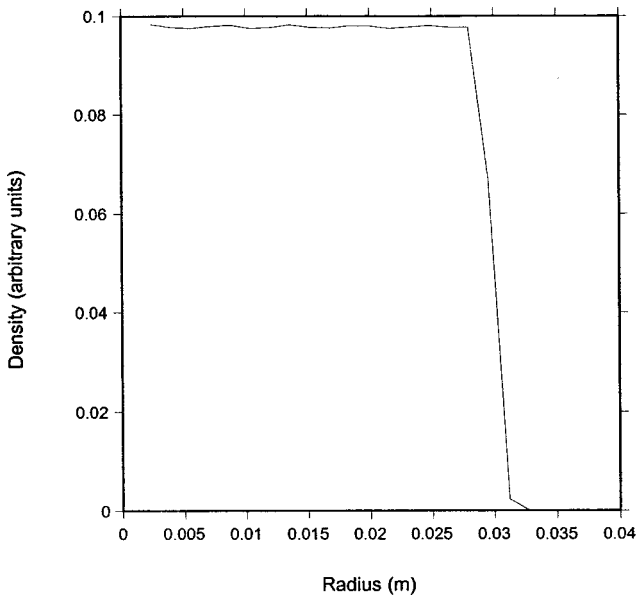

FIG. 1. Ion density distribution after 1 nsec.

origin (the fluid momentum tends to average to zero at the origin in a strict fluid model) and was used for this study.

In Fig. 1, we plot the ion density as a function of radial position after 1 nsec of an electron beam that is 3 cm in radius and of uniform radial and axial density, using hydrogen ions. We see that the ion density is still uniform. In Fig. 2, we plot the ion density after 10 nsec of the electron beam. We now see that the ion density is moving toward the center as particles at the initial time are reaching a quarter of their oscillation period. At 20 nsec (Fig. 3), the ion distribution is already close to the equilibrium distribution, even though this time is only at about 36% of the oscillation period. For heavier ions, this time would be longer, but the ion distribution would also approach the equilibrium distribution at about one-third of the oscillation period. It is also important

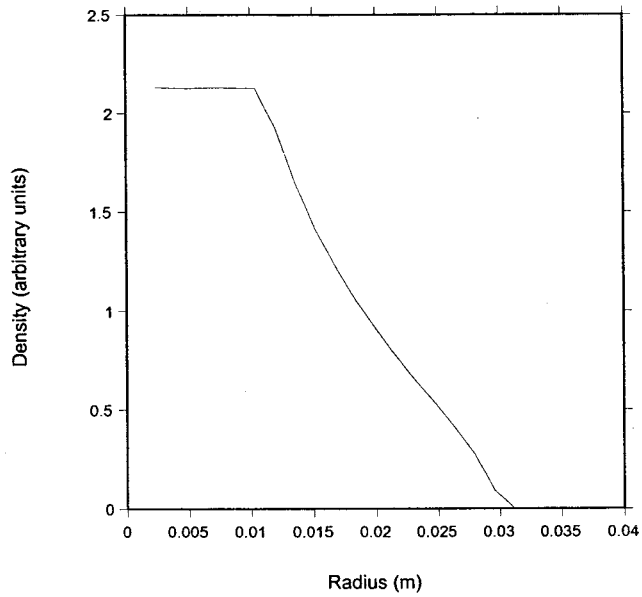

FIG. 2. Ion density distribution after 10 nsec.

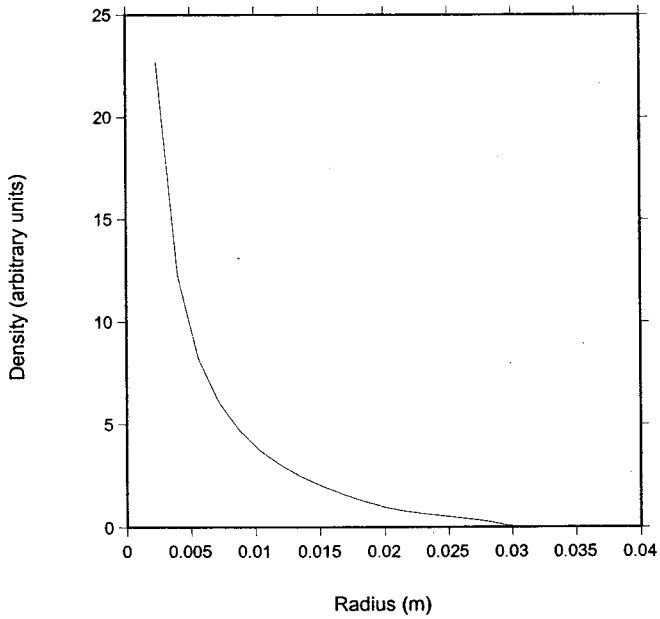

FIG. 3. Ion density distribution after 20 nsec (36% of the oscillation period).

to note that a spread of ion masses would tend to help the distribution reach its equilibrium form earlier. Note that in Fig. 3, some small kinks in the distribution is seen due to the coarseness of the electron bunch slices (0.56 nsec apiece).

We see that by 200 nsec the distribution is smoother (Fig. 4), and by 500 nsec (Fig. 5) excellent agreement with the analytic equilibrium distribution function is reached. Note that this equilibrium distribution will be reached in about 100 nsec for a nitrogen gas for a 3-cm, 2-kA electron beam, and in much less time for smaller radius electron beams.

Recall that this equilibrium distribution was found for the case the self-fields from the ions can be ignored. The singu-

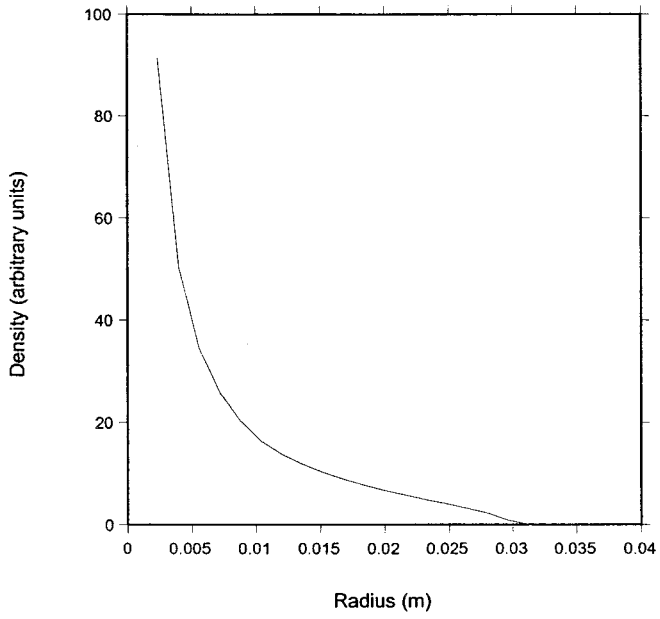

FIG. 4. Ion density distribution after 200 nsec.

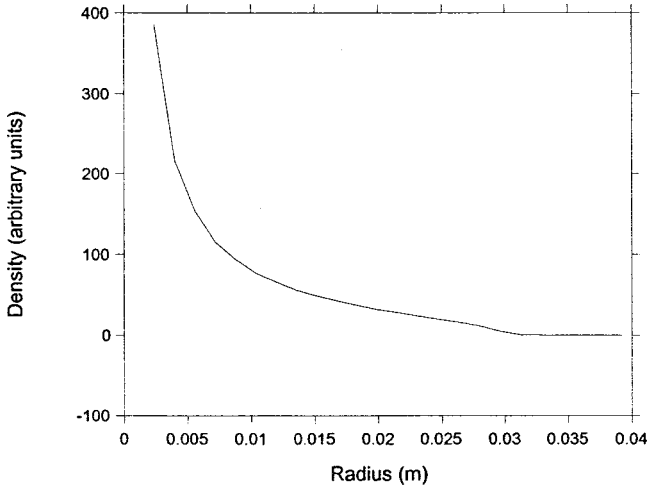

FIG. 5. Ion density distribution after 500 nsec (solid line) and analytic equilibrium distribution [Eq. (9)] (circles).

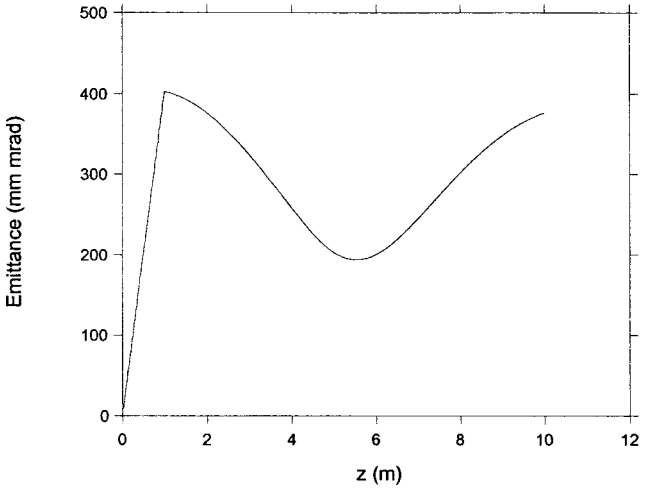

FIG. 6. Slice emittance of the final slice in the electron bunch as a function of axial location. Note the rapid emittance growth in the high pressure region (0–1 m), followed by emittance oscillations.

larity at the origin for the equilibrium distribution leads to an infinite force there, distorting the actual equilibrium distribution there, as described earlier. However, the amount of charge at the origin is small, and the distortion will be in a region limited close to the origin for small ionization fractions. The effect on the electron optics will be likewise limited to near the origin, affecting only few electrons and those with the least impact on the overall beam emittance.

III. EMITTANCE GROWTH IN THE LINEAR REGIME

There are two possible effects from the forces induced by the electric field on the ions that can produce an emittance growth in the electron beam. For very short electron bunch lengths, there is a time-dependent focusing effect, that is linear if the beam distribution is uniform. For long electron bunch lengths, the focusing force is always nonlinear. Both effects can lead to an emittance growth for the entire bunch, although the first effect will tend not to increase the emittance of individual electron bunch slices. However, even for the short-bunch case, if the focusing force is large enough to change the radius of the latter part of the electron bunch significantly, the time-dependent focusing force will be nonlinear.

The normalized, 90% emittance of the electron beam, defined here as

$$\varepsilon = 2\gamma\beta\sqrt{\langle r^2\rangle\langle r'^2\rangle - \langle rr'\rangle^2}, \tag{9}$$

is an accurate measure of the beam quality for many types of applications, where the brackets indicate an ensemble average (including axial position within the electron bunch), and the prime refers to an axial derivative. The radial force from the equilibrium ion density on an electron in the bunch for the uniform-density case is given by

$$F_{r,\mathrm{ion}}(r,t) = \frac{2en_e n_g \sigma c}{\varepsilon_0 r \pi a^2} t\left(a^2 \sin^{-1}\frac{r}{a} + a\sqrt{a^2 - r^2}\right), \tag{10}$$

which is clearly nonlinear and will cause both an overall and a slice emittance growth.

For studying the slice emittance and overall emittance growth, we simulate an initially uniform electron bunch traversing first a short region (1 m long) of relatively high gas pressure followed by a longer region (4 m long) with very low gas pressure. This is done because the emittance growth in the higher gas region starts emittance oscillations coupled to transverse plasma oscillations (or space-charge waves), and that the emittance growth is minimized at about 5 m (see Fig. 6). At that location, much of the excess kinetic energy associated with the emittance growth is transferred to excess potential energy—or, in other words, at 5 m the radial electron beam distribution is as nonuniform as it will became. Each electron slice is distributed with 8000 macroelectrons.

In Fig. 7 we plot the final slice emittance at 5 m as we change the electron bunch length and pressure, but keeping the product constant (so the total ionization is kept constant). The slice emittance is a strong measure of how long if takes the ion distribution to reach equilibrium, about 300 nsec.

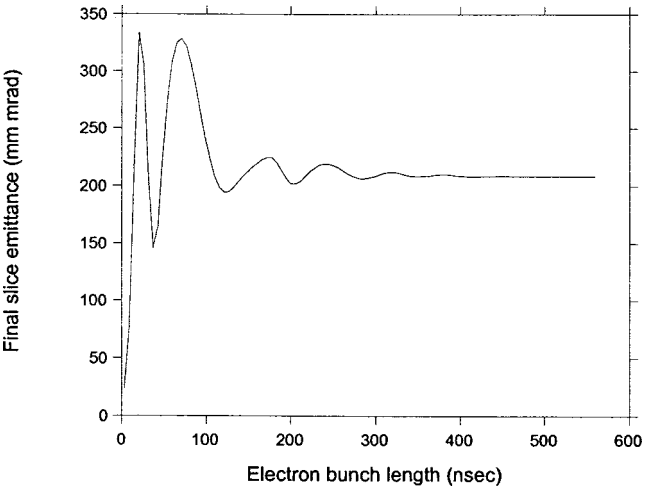

FIG. 7. Final slice emittance as a function of the electron bunch length.

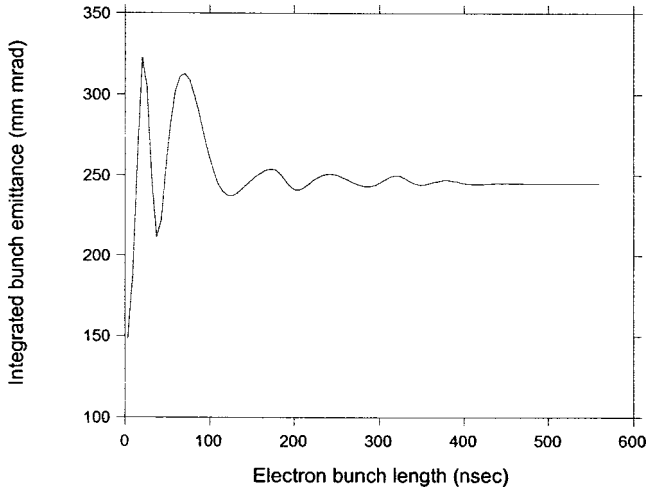

FIG. 8. Integrated bunch emittance as a function of the electron bunch length.

In Fig. 8, we plot the integrated bunch emittance as a function of electron bunch length. Note that the integrated bunch emittance mirrors the final slice emittance to a good degree. This indicates that for long electron bunches >100 nsec, the overall emittance is dominated by the increase in slice emittance, and not just a differential rotation in phase space among the different bunch slices (which accounts for the initial emittance of 150 mm mrad). In Fig. 9, we plot the final slice emittance as a function of final ionization, for an interaction length of 0.1 m.

From Fig. 9, we can determine the linear emittance growth rate, which is very nearly

$$\varepsilon = 0.155 l f_{\text{final}}, \tag{11}$$

where l is the interaction length, and f_{final} is the final fractional ionization at the end of the electron pulse. Numerical simulations show that this emittance growth is mostly linear with fractional ionization, even for thick length l's.

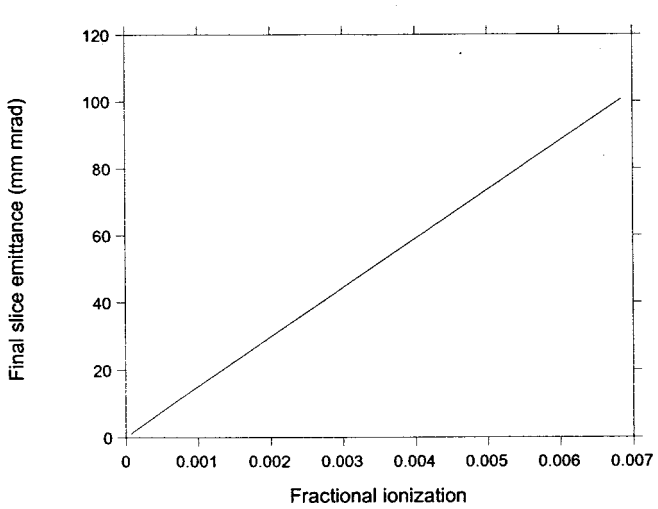

FIG. 9. Slice emittance from a short region of high gas pressure vs gas pressure.

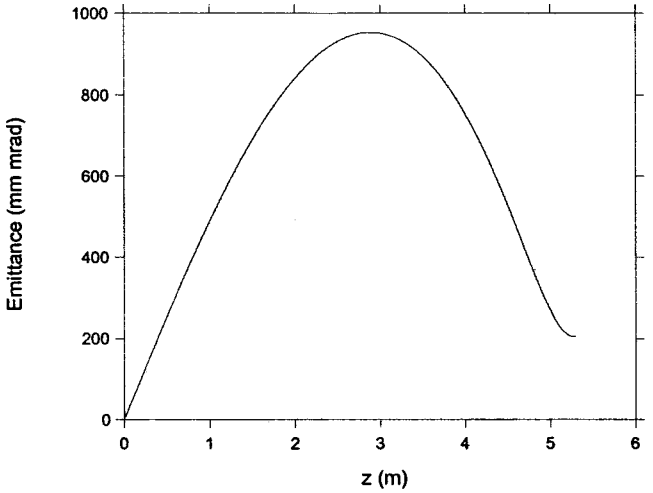

FIG. 10. Emittance oscillation for an initially nonuniform-density electron beam.

IV. NONLINEAR EMITTANCE GROWTH

It is well known that a zero-emittance, uniform-density electron beam will have minor emittance growth, if any, but an initially nonuniform electron beam can have large emittance growth [8] because the initial beam distribution is not an equilibrium one. However, this emittance growth will lead to emittance oscillations, as shown in Fig. 6. If the initial emittance is due to a nonequilibrium beam density, the emittance will grow as the beam density approaches the equilibrium shape, and then will decrease as the density becomes nonequilibrium again [9]. In practical accelerators, diode focusing and nonlinear focusing effects will lead to nonequilibrium density distributions. Most high-brightness accelerator designs account for this, and adjust the focusing so that the final accelerator application occurs at one of the emit-

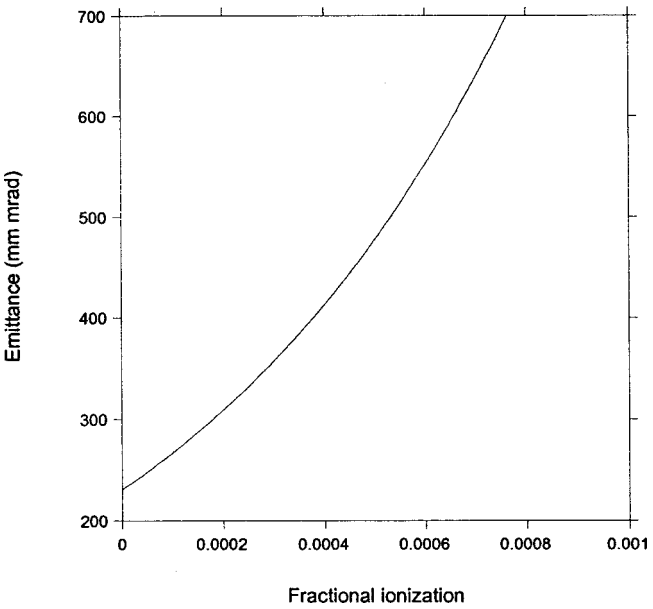

FIG. 11. Slice emittance growth at the emittance oscillation minimum, as a function of final fractional ionization.

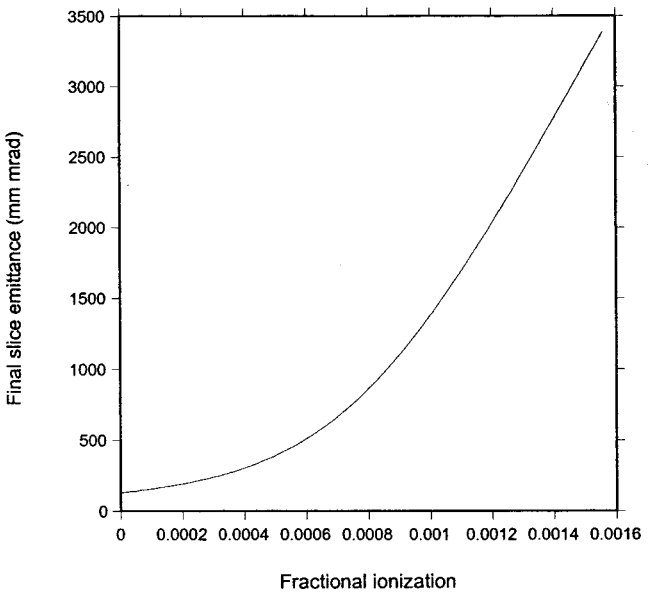

FIG. 12. Emittance growth as a function of final fractional ionization for the DARHT long-pulse accelerator.

tance minimums (an integral number of half-transverse plasma oscillations) [10,11]. In Fig. 10 we show one emittance oscillation for an initially partially hollow, 2-kA, 5-MeV electron beam with a 3-cm radius. The emittance, initially zero, grows to nearly 1000 mm mrad, before dropping down to 205 mm mrad, at an axial location of 5.3 m. The focusing magnetic field is adjusted so the rms beam size remains constant over this length.

For this case, slight focusing changes will tend to spoil the complete emittance oscillation, by slightly changing the period of the transverse plasma oscillation. The emittance oscillation obeys a sinusoidal function [9,11], and thus is locally quadratic near its minimum in terms of either axial position or focusing strength. We would then expect that the additional focusing from residual gas ionization will make the slice emittances grow quadratically with fractional ionization. In Fig. 11, we plot the growth of the final slice emittance at the end of the nominal emittance oscillation (5.3 m) as a function of final fractional ionization.

This complex coupling between ionization and transverse plasma oscillations is seen in simulations of actual beamlines. In Fig. 12, we plot the simulated emittance of the DARHT second axis accelerator as a function of residual-gas final ionization. As in Fig. 11, the emittance growth is quadratic. The maximum acceptable emittance for this machine is about 1000 mm mrad, or a final fractional ionization of about 0.001. For a typical cross section of $\sigma = 2(10^{-18})\ \mathrm{cm}^{-2}$ and an electron pulse length of 2 μs (the electron pulse length in the DARHT long-pulse accelerator), this leads to a maximum acceptable residual gas pressure of $P_g = 2.5(10^{-7})$ torr. This residual gas pressure is certainly achievable, but not luxurious.

V. CONCLUSION

We have presented a model for ionized gas motion within an electron beam. For long-pulse lengths, the ions mostly reach an equilibrium distribution in less than one-half of an oscillation period. This equilibrium distribution is highly nonuniform, and leads to both slice and axially integrated emittance growth. We have also seen that the coupling between the time-dependent ion focusing and emittance oscillations in practical accelerator designs leads to a quadratic scaling of the emittance growth with respect to final fractional ionization, for long pulse lengths, and puts upper limits on allowable residual gas pressures for new, long-pulse, high-brightness electron accelerators.

ACKNOWLEDGMENT

This work was supported by funds from the DARHT project at Los Alamos National Laboratory, operated by the University of California for the U.S. Department of Energy.

[1] H. L. Buchanan, Phys. Fluids **30**, 221 (1987).
[2] E. P. Lee, Phys. Fluids **21**, 1327 (1978).
[3] T. O. Raubenheimer and F. Zimmermann, Phys. Rev. E **52**, 5487 (1995); G. V. Stupakov, T. O. Raubenheimer, and F. Zimmermann, *ibid.* **52**, 5499 (1995).
[4] J. Byrd, A. Chao, S. Heifits, M. Minty, T. O. Raubenheimer, J. Seeman, G. Stupakov, J. Thomson, and F. Zimmermann, Phys. Rev. Lett. **79**, 79 (1997).
[5] G. J. Caporaso and J. F. McCarrick (unpublished).
[6] M. Reiser, *Theory and Design of Particle Beams* (Wiley, New York, 1994).
[7] M. J. Burns, B. E. Carlsten, T. J. T. Kwan, D. C. Moir, D. S. Prono, S. A. Watson, E. L. Burgess, H. L. Rutkowski, G. J. Caporaso, Y. J. Chen, S. Sampayan, and G. Westenskow, *DARHT Accelerators Update and Plans for Initial Operation*, Proceedings of 1999 Particle Accelerator Conference, New York, 1999 (IEEE, Piscataway, NJ, 1999).
[8] B. E. Carlsten, Phys. Rev. E **58**, 2489 (1998).
[9] B. E. Carlsten, Phys. Rev. E **60**, 2280 (1999).
[10] B. E. Carlsten, Phys. Plasmas **6**, 3615 (1999).
[11] S. G. Anderson and J. B. Rosenzweig, Phys. Rev. ST Accel. Beams **3**, 094201 (2000).